J|A|C|S ARTICLES

Published on Web 12/05/2008

Fast Amide Proton Exchange Reveals Close Relation between Native-State Dynamics and Unfolding Kinetics

Hagen Hofmann,*,† Ulrich Weininger,‡ Christian Löw,‡ Ralph P. Golbik,† Jochen Balbach,‡ and Renate Ulbrich-Hofmann*,†

Institute of Biochemistry and Biotechnology, Institute of Physics, Biophysics group and Mitteldeutsches Zentrum für Struktur and Dynamik der Proteine (MZP), Martin-Luther University Halle-Wittenberg, 06099 Halle

Received July 4, 2008; E-mail: h.hofmann@bioc.uzh.ch

Abstract: It has long been recognized that many proteins fold and unfold via partially structured intermediates, but it is still unclear why some proteins unfold in a two-state fashion while others do not. Here we compare the unfolding pathway of the small one-domain protein barstar with its dynamics under native conditions. Using very fast proton-exchange experiments, extensive dynamic heterogeneity within the native-state ensemble could be identified. Especially the dynamics of helix 3, covering the hydrophobic core of the molecule, is found to be clearly cooperative but decoupled from the global dynamics. Moreover, an initial unfolding of this helix followed by the breakdown of the remaining tertiary structure can be concluded from the comparison of the proton exchange experiments with unfolding kinetics detected by stopped-flow fluorescence. We infer that the unfolding pathway of barstar is closely coupled to its native-state dynamics.

1. Introduction

Protein folding reactions often appear deceptively simple. Typically for single-domain proteins only two states are supposed to exist at equilibrium, the folded native state and the featureless unfolded state.[1] The two-state approximation assumes native and unfolded molecules to be discrete and homogeneous states. However, due to the chemical and structural complexity of proteins the two-state model must be a very rough approximation. Indeed, kinetic experiments show that many, even small proteins such as lysozyme[2−5] and ribonuclease A,[6,7] fold via transiently populated intermediates. In such cases, the two-state approximation is not applicable and more sophisticated models[8] are needed. In general, ground and even transition states of proteins represent ensembles of rapidly fluctuating species on a high-dimensional energy landscape rather than distinct homogeneous states.[9−14] Heterogeneities in the native[15] or unfolded state[16−18] due to *cis*−*trans* isomerization of peptidyl−prolyl bonds were already shown to result in complex folding and unfolding kinetics. Importantly, if the dynamics in one of two ground states (native or unfolded state) are much faster than the transitions between these states, the ground states can be considered as homogeneous thermodynamic states. However, as soon as the intrinsic dynamics of the ground states are similar or slower than the transitions between these states, they can strongly influence the protein folding and unfolding pathways. Under these conditions, the cooperative unfolding of a protein might be kinetically coupled to the dynamics of its native-state ensemble.

Experimentally, site-resolved information on the native-state dynamics of proteins can be obtained by H/D exchange experiments coupled with NMR spectroscopy.[19] However, this method is usually limited to exchange kinetics in the time range of hours, whereas the time range of seconds and milliseconds remains, with a few exceptions,[20−23] unexplored by this method. The pseudowildtype variant P27A/C40A/C82A (pWT) of

† Institute of Biochemistry and Biotechnology.
‡ Institute of Physics.

(1) Jackson, S. E. *Fold. Des.* **1998**, *3*, R81–91.
(2) Kuwajima, K.; Hiraoka, Y.; Ikeguchi, M.; Sugai, S. *Biochemistry* **1985**, *24*, 874–881.
(3) Chaffotte, A. F.; Guillou, Y.; Goldberg, M. E. *Biochemistry* **1992**, *31*, 9694–9702.
(4) Radford, S. E.; Dobson, C. M.; Evans, P. A. *Nature* **1992**, *358*, 302–307.
(5) Itzhaki, L. S.; Evans, P. A.; Dobson, C. M.; Radford, S. E. *Biochemistry* **1994**, *33*, 5212–5220.
(6) Kiefhaber, T.; Baldwin, R. L. *Proc. Natl. Acad. Sci. U.S.A.* **1995**, *92*, 2657–2661.
(7) Schmid, F. X. *Biochemistry* **1983**, *22*, 4690–4696.
(8) Ikai, A.; Tanford, C. *J. Mol. Biol.* **1973**, *73*, 145–163.
(9) Bryngelson, J. D.; Wolynes, P. G. *Proc. Natl. Acad. Sci. U.S.A.* **1987**, *84*, 7524–7528.
(10) Leopold, P. E.; Montal, M.; Onuchic, J. N. *Proc. Natl. Acad. Sci. U.S.A.* **1992**, *89*, 8721–8725.
(11) Onuchic, J. N.; Wolynes, P. G.; Luthey-Schulten, Z.; Socci, N. D. *Proc. Natl. Acad. Sci. U.S.A.* **1995**, *92*, 3626–3630.
(12) Baldwin, R. L. *Nature* **1994**, *369*, 183–184.
(13) Baldwin, R. L. *J. Biomol. NMR* **1995**, *5*, 103–109.
(14) Dill, K. A.; Chan, H. S. *Nat. Struct. Biol.* **1997**, *4*, 10–19.
(15) Jakob, R.; Schmid, F. X. *J. Mol. Biol.* **2008**, *377*, 1560–1575.
(16) Golbik, R.; Fischer, G.; Fersht, A. R. *Protein Sci.* **1999**, *8*, 1505–15014.
(17) Schreiber, G.; Fersht, A. R. *Biochemistry* **1993**, *32*, 11195–11203.
(18) Shastry, M. C.; Agashe, V. R.; Udgaonkar, J. B. *Protein Sci.* **1994**, *3*, 1409–1417.
(19) Bai, Y.; Sosnick, T. R.; Mayne, L.; Englander, S. W. *Science* **1995**, *299*, 192–197.
(20) Hoang, L.; Bedard, S.; Krishna, M. G. M.; Lin, Y.; Englander, S. W. *Proc. Natl. Acad. Sci. U.S.A.* **2002**, *99*, 12173–12178.
(21) Krishna, M. G. M.; Lin, Y.; Mayne, L.; Englander, S. W. *J. Mol. Biol.* **2003**, *334*, 501–513.
(22) Meisner, K. W.; Sosnick, T. R. *Proc. Natl. Acad. Sci. U.S.A.* **2004**, *101*, 15639–15639.
(23) Rodriguez, H. M.; Robertson, A. D.; Gregoret, L. M. *Biochemistry* **2002**, *41*, 2140–2148.

 10.1021/ja8048942 CCC: $40.75

barstar,[16] a single-domain protein containing 90 amino acid residues, has a highly dynamic native structure.[24,25] Even in the more stable barstar-WT the majority of backbone amide protons were shown to exchange against deuterium during the dead time of several minutes.[26] Therefore, studies of the native-state dynamics on a residue-by-residue level have been limited so far to the nanoseconds-to-picoseconds time range.[27] In contrast, the folding pathway of this protein has been extensively studied and was shown to occur in the microseconds to seconds time domain.[28,29] A detailed analysis of burst phase amplitudes revealed that barstar unfolds via two intermediates that are transiently populated on parallel pathways.[30]

In the present work a very fast proton exchange approach different from conventional H/D exchange and hitherto mostly applied to peptides and unfolded proteins[31−33] allowed the detection of proton exchange kinetics in the millisecond time regime. Moreover, the urea induced unfolding transition of barstar-pWT was analyzed at residue resolution by ^{15}N-TROSY-HSQC spectra. A close kinetic coupling between the native-state dynamics and the unfolding reaction of barstar-pWT can be derived from the comparison of the proton exchange kinetics with the unfolding kinetics detected by fluorescence stopped-flow experiments.

2. Results

2.1. Urea Induced Unfolding Transitions Detected by 2D ^{15}N-TROSY-HSQC Spectra. Despite its complex folding and unfolding kinetics, differential scanning calorimetry (DSC) revealed that the unfolding of barstar in equilibrium fits the two-state model.[34] Two-state transitions were also found in our experiments following the urea induced unfolding via the resonances of 48 backbone amides in 2D ^{15}N-TROSY-HSQC spectra. Examples of the obtained transition curves are shown in Figure 1A. Presuming a two-state transition, the free energy of unfolding $\Delta G°(H_2O)$, the cooperativity m_{eq}, and the urea concentration at the transition midpoint $[urea]_{1/2}$ were calculated for all individual transitions. A random scatter of the obtained parameters around their mean values ($\langle m_{eq}\rangle = 4.6 \pm 0.4$ kJ·mol^{-1}·M^{-1}, $\langle[urea]_{1/2}\rangle = 2.66 \pm 0.18$ M, $\langle\Delta G°(H_2O)\rangle = 12.1 \pm 1.6$ kJ mol^{-1}) was observed (Figure 1B; Supporting Information, Table S1). Inversely, each of the experimentally determined transitions could be well fitted using the mean stability parameters. Hence, assuming a transition between two homogeneous ground states (N and U) is sufficient to describe the unfolding of barstar-pWT at equilibrium.

2.2. Native-State Proton Exchange. 2.2.1. Principle of Measurement. Spontaneous structural fluctuations as well as local and global unfolding events allow an exchange of the amide protons by solvent protons. The exchange is defined by an opening rate constant k_{op} and a closing rate constant k_{cl}. At pH > 4 this process is base catalyzed and occurs according to

$$\mathbf{C} \underset{k_{cl}}{\overset{k_{op}}{\rightleftharpoons}} \mathbf{O} \xrightarrow{k_{int}[OH^-]} \mathbf{O_{ex}} \quad (1)$$

with **C** corresponding to the closed state not accessible to proton exchange, **O** to the opened state, competent for protein exchange, $\mathbf{O_{ex}}$ to the amide proton exchanged state, and k_{int} to the intrinsic exchange rate constant of the freely accessible amide proton.[35−38] The observed exchange rate constant (k_{HX}) is given by the Linderstrøm−Lang expression

$$k_{HX} = \frac{k_{op} \cdot k_{int} \cdot [OH^-]}{k_{op} + k_{cl} + k_{int} \cdot [OH^-]} \quad (2)$$

In the case of the so-called EX1 limit with $(k_{op} + k_{cl}) \ll k_{int}[OH^-]$, every opening event leads to a proton exchange and eq 2 reduces to $k_{HX} = k_{op}$. In contrast, in the EX2 limit where $k_{cl} \gg (k_{op} + k_{int}[OH^-])$, an equilibrium between the closed and open forms is established with the equilibrium constant $K_{eq} = k_{op}/k_{cl} = k_{HX}/(k_{int}[OH^-])$. The knowledge of the intrinsic rate constant (k_{int})[37,38] allows the calculation of K_{eq} and hence the calculation of the free energy change via $\Delta G_{HX} = -RT \ln K_{eq}$. Therefore, the determination of k_{HX} at different pH values spanning the EX2 and EX1 limits allows the determination of k_{op}, k_{cl}, and K_{eq}.

This type of analyses necessarily assumes that the stability of the protein is not affected by the change in the considered pH range. To check the validity of this assumption for barstar-pWT we determined its thermodynamic stability as a function of the pH by far UV-CD and fluorescence spectroscopy. Between pH 6.5 and 10.0 virtually no change, neither in the fluorescence and CD signals nor in the resulting $\Delta G°(H_2O)$ values, could be detected as demonstrated in the Supporting Information (Figure S1A and B). In addition, the rate constants for refolding and unfolding were shown to be similar at pH 8.0, 9.0, and 10.0 (Figure S1C).

A modified variant of the MEXICO (*measurement of fast proton exchange rates in isotopically labeled compounds*) pulse sequence for ^{15}N labeled proteins[31−33] was used to record the proton exchange kinetics of barstar-pWT in the millisecond time range at five different pH values (6.5, 7.0, 8.0, 9.0, and 10.0). The method determines the back-exchange of water protons to the backbone amide after dephasing the amide proton magnetization by pulse-field gradients. Examples of 2D ^{1}H−^{15}N correlation spectra after different exchange times and representative exchange kinetics are shown in the Supporting Information (Figure S2A and B). For 44 amide protons the observed rate constants (k_{HX}) of the proton exchange were independent of the pH (Figure 2B, Table S2), indicating an exchange via the EX1 mechanism. In contrast, for 20 amide protons a switch from EX2 to EX1 was observed (Figure 2A and C, Table S2).

2.2.2. Opening Rate Constants. In total, k_{op} for 64 amino acid residues could be determined (Figure 3A). This corresponds to 70% of all residues of the protein and gives a representative overview of the distribution of k_{op} along the sequence. Surpris-

(24) Wong, K. B.; Daggett, V. *Biochemistry* **1998**, *37*, 11182–11192.
(25) Li, H.; Frieden, C. *Biochemistry* **2007**, *46*, 4337–4347.
(26) Bhuyan, A. K.; Udgaonkar, J. B. *Proteins* **1998**, *30*, 295–308.
(27) Wong, K.; Fersht, A.; Freund, S. M. V. *J. Mol. Biol.* **1997**, *268*, 494–511.
(28) Nölting, B.; Golbik, R.; Neira, J. L.; Soler-Gonzalez, A. S.; Schreiber, G.; Fersht, A. R. *Proc. Natl. Acad. Sci. U.S.A.* **1997**, *94*, 826–830.
(29) Shastry, M. C.; Udgaonkar, J. B. *J. Mol. Biol.* **1995**, *247*, 1013–1027.
(30) Zaidi, F. N.; Nath, U.; Udgaonkar, J. B. *Nat. Struct. Biol.* **1997**, *4*, 1016–1024.
(31) Koide, S.; Jahnke, W.; Wright, P. E. *J. Biomol. NMR* **1997**, *6*, 306–312.
(32) Mori, S.; van Zijl, P. C.; Shortle, D. *Proteins* **1997**, *28*, 325–332.
(33) Gemmecker, G.; Jahnke, W.; Kessler, H. *J. Am. Chem. Soc.* **1993**, *115*, 11620–11621.
(34) Schöppe, A.; Hinz, H. J.; Agashe, V. R.; Ramachandran, S.; Udgaonkar, S. B. *Protein Sci.* **1997**, *6*, 2196–2202.
(35) Linderstrøm-Lang, K. *Chem. Soc. Spec. Publ.* **1955**, *2*, 1–20.
(36) Hvidt, A.; Nielsen, S. O. *Adv. Protein Chem.* **1966**, *21*, 287–386.
(37) Bai, Y.; Milne, J. S.; Mayne, L.; Englander, S. W. *Proteins* **1993**, *17*, 75–86.
(38) Connelly, G. P.; Bai, Y.; Jeng, M. F.; Englander, S. W. *Proteins* **1993**, *17*, 87–92.

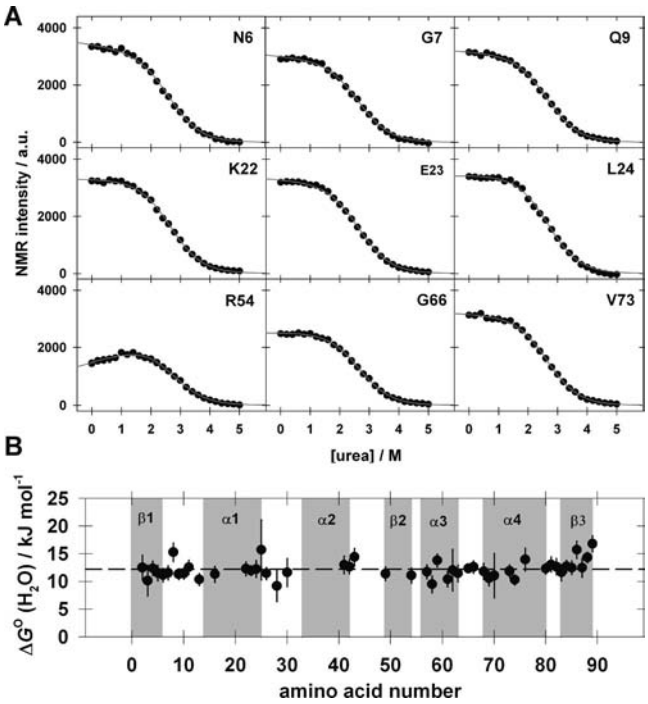

Figure 1. Urea induced unfolding detected by NMR spectroscopy. (A) Examples of transition curves for different amino-acid residues as derived from the cross-peak intensities of 2D ^{15}N-HSQC-TROSY spectra. (B) $\Delta G°(H_2O)$ calculated from the unfolding transitions of the single amino acid residues. Error bars indicate the standard deviations derived from the fit according to the two-state model. Gray bars represent the indicated secondary structure elements.

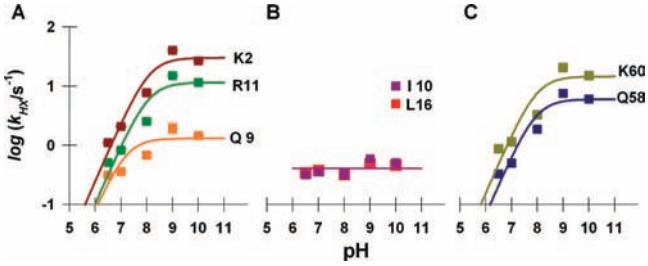

Figure 2. Rate constants of native-state proton exchange (k_{HX}) for selected amino acid residues as a function of pH. (A) Amide protons showing a switch from EX2 to EX1 mechanism. (B) Amide protons exchanging via the EX1 mechanism over the whole pH range measured. (C) Examples of amide protons from helix 3. The solid lines are fittings according to eq 2 with k_{int} calculated as described in refs 37 and 38.

ingly, k_{op} values vary by more than 2 orders of magnitude ($0.2-40$ s^{-1}). High opening rate constants were found in the loops 1 and 2, at the N-terminus, and especially in the region including the residues 58 to 68 (in helix 3 and the adjacent loop). An asymmetric distribution with at least two populations of residues showing opening rate constants of 0.3 and $2-10$ s^{-1} is obtained when plotting the opening rate constants in a histogram (Figure 3C).

2.2.3. Closing Rate Constants. The rate constants k_{cl} obtained for the amide protons showing an exchange mechanism switching from EX2 to EX1 (Figure 3B) range from 10 s^{-1} ($\tau = 100$ ms) to 2000 s^{-1} ($\tau = 500$ μs) thus spanning again more than 2 orders of magnitude. Low k_{cl} values are found in the loops 1, 2, and 6 when relating the k_{cl} values to the secondary structure of barstar-pWT. In contrast, the helices 3 and 4, the N-terminal beta-sheet (β1), and loop 5 show very large closing rate constants, up to the microsecond time range (Figure 3B). A summary of the obtained k_{cl} values in a histogram (Figure 3D)

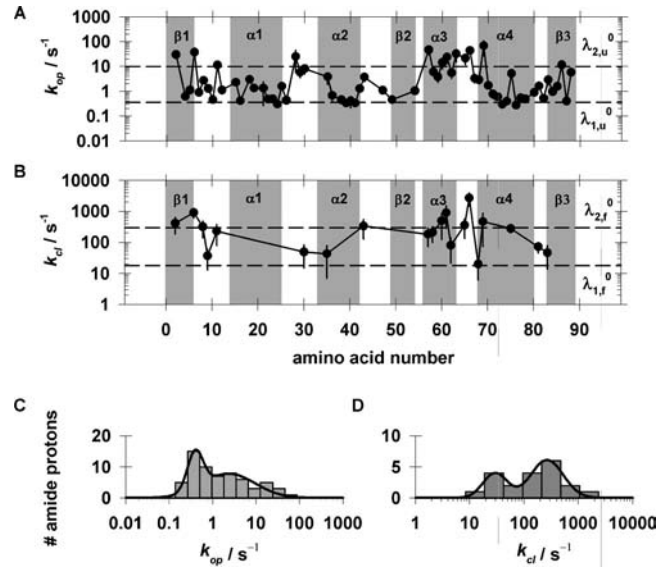

Figure 3. Rate constants for the opening (k_{op}) and closing (k_{cl}) reactions. (A and B) k_{op} and k_{cl} plotted against the amino acid number. Error bars give the standard deviations resulting from the fit according to eq 2. Dashed lines correspond to the folding ($\lambda_{1,f}^0$ and $\lambda_{2,f}^0$) and unfolding ($\lambda_{1,u}^0$ and $\lambda_{2,u}^0$) rate constants under native conditions determined by stopped-flow fluorescence (see also Figure 6). (C and D) Histograms of k_{op} and k_{cl}.

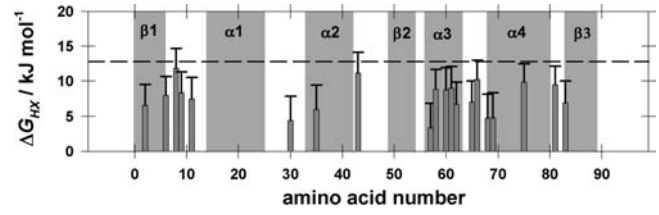

Figure 4. Gibbs free energy difference (ΔG_{HX}) between the opened and closed states. The dashed line represents the free energy derived from the NMR-detected urea transitions (Figure 1).

shows roughly two populations of residues with mean rate constants of 300 s^{-1} and $10-30$ s^{-1}, respectively.

2.2.4. Free Energy Differences between Opened and Closed State. For all amide protons that exchange via the EX2 limit, the free energy change ΔG_{HX} between the opened and closed state could be calculated (Figure 4). Only two residues, E8 ($\Delta G_{HX} = 11.8 \pm 2.9$ kJ·mol^{-1}) and G43 ($\Delta G_{HX} = 11.2 \pm 2.9$ kJ·mol^{-1}), show ΔG_{HX} values close to the free energy for unfolding ($\langle \Delta G°(H_2O) \rangle = 12.1 \pm 1.6$ kJ·mol^{-1}) determined by 2D ^{15}N-TROSY-HSQCs (see above). The remaining 18 residues show significant lower ΔG_{HX} values indicating that local processes instead of global unfolding contribute to the proton-exchange kinetics.

2.3. Folding and Unfolding Kinetics of Barstar-pWT Followed by Stopped-Flow Fluorescence. Barstar-pWT contains three tryptophan residues. Two of them are exposed to the solvent (W38, W44), whereas W53 is buried in the hydrophobic core of the protein (Figure 7). The change in fluorescence intensity upon unfolding was shown to result predominantly from W53, which becomes solvent-accessible during unfolding.[30] Therefore, the fluorescence of W53 is a sensitive probe for the global unfolding process of this protein. Structurally, W53 is in close proximity to helix 3, which has been shown to consist of residues with very high k_{op} values (Figure 3A). Using urea as a denaturant, two phases could be detected in the unfolding kinetics measured in a stopped-flow fluorescence instrument (Figure 5A). The main unfolding reaction gives an unfolding rate constant (λ_1) of 2.01 $\pm$ 0.01 s^{-1} at 6.6 M urea,

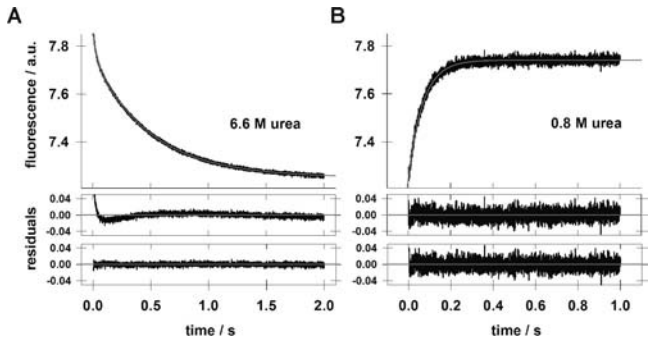

Figure 5. Unfolding and refolding kinetics of barstar-pWT followed by stopped-flow fluorescence spectroscopy. (A) Unfolding kinetics at 6.6 M urea. (B) Refolding kinetics at 0.8 M urea starting from the unfolded molecules having the Y47−P48 bond in a *cis*-conformation (U_{cis}). U_{cis} was achieved by unfolding the protein for 3 s in 4.3 M urea prior to the refolding reaction. The residuals for the single and double exponential fit are shown in the upper and lower panels.

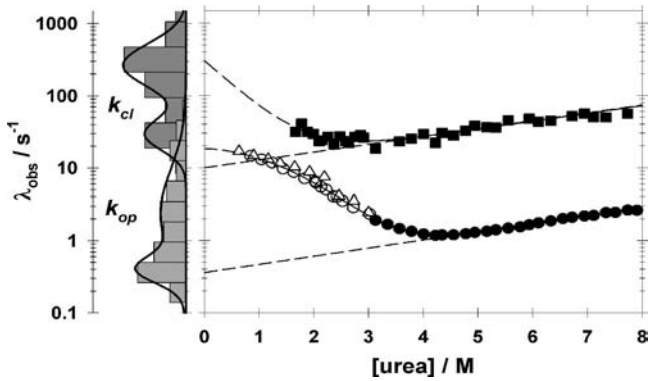

Figure 6. Chevron plot for barstar-pWT in comparison with the opening and closing rate constants. λ_1 (●) and λ_2 (■) as determined from unfolding experiments as well as λ_1 as determined from refolding experiments starting from U_{cis} (○) and starting from the equilibrium mixture of U_{cis} and U_{trans} (△) as function of the urea concentration. Solid lines are fits according to eqs 4 and 5. Dashed lines are extrapolations to 0 M urea. Histograms of k_{op} (light gray) and k_{cl} (dark gray) were taken from Figure 3C and D and normalized to an area of 1.

whereas the second, fast unfolding reaction gives a rate constant (λ_2) of 34.0 ± 0.5 s^{-1} at 6.6 M urea. Obviously, barstar-pWT unfolds via at least one intermediate, even at high urea concentrations. In contrast, only one folding reaction is observed (Figure 5B) irrespective of starting from the unfolded protein with Y47−P48 in the *cis*-conformation (U_{cis}) or from an equilibrium mixture of U_{cis} and U_{trans} with U_{trans} being the unfolded protein with Y47−P48 in the *trans*-conformation (Figure 6). These folding and unfolding kinetics imply that the unfolding intermediate is either obligatory with the rate-limiting step being the transition between the intermediate and the unfolded molecules or populated on a parallel pathway in addition to the global unfolding transition. The amplitude of λ_2 was found to be small (10%) and independent of the urea concentration (data not shown). Due to the latter fact, it is very unlikely that the intermediate is populated on-pathway since this would necessarily lead to a change in the amplitude with the urea concentration.

Figure 6 shows λ_1 and λ_2 for barstar-pWT as a function of the urea concentration. The histograms for the opening and closing rate constants of the individual amide protons obtained from the HX experiments (Figure 3C and D) are additionally shown for comparison. Remarkably, the extrapolation of the unfolding branch of λ_1 and λ_2 from high urea concentrations to native conditions results in values ($\lambda_{1,u}^0 = 0.36 \pm 0.04$ s^{-1} and $\lambda_{2,u}^0 = 9.9 \pm 1.2$ s^{-1}) that coincide with the k_{op} values of the two main fractions of amide protons in HX exchange (Figure 6). Similarly, the rate constants for folding under native conditions ($\lambda_{1,f}^0$ and $\lambda_{2,f}^0$) can be related to the k_{cl} values. At <2 M urea the logarithm of λ_1 clearly changes nonlinear with the urea concentration, attaining a rate constant of $\lambda_{1,f}^0 = 18.0 \pm 0.8$ s^{-1} at 0 M urea (Figure 6). This value corresponds to the population of amide protons with k_{cl} values around 10−30 s^{-1}. In the unfolding experiments, λ_2 increases with decreasing urea concentration at <3 M urea, indicating that under these conditions λ_2 is dominated by the microscopic rate constants of refolding. The extrapolation of the folding branch of the fast phase yields a rate constant for folding of $\lambda_{2,f}^0 = 296 \pm 224$ s^{-1} at 0 M urea. Despite the large error resulting from the extrapolation over the broad range from 1.5 to 0 M urea, this value is in the same order of size as the k_{cl} values obtained from the proton exchange experiments (Figure 6).

3. Discussion

As concluded from 48 transition curves for the urea induced unfolding of barstar-pWT, the free energy of unfolding amounts to $\Delta G°(H_2O) = 12.1 \pm 1.6$ kJ mol^{-1} (Figure 1), irrespective of which amide proton signal in the ^{15}N-TROSY-HSQC spectra is used to follow the transition. Hence, a two-state model sufficiently explains the unfolding of barstar-pWT in equilibrium. Accordingly, in a recent single-molecule study only native and unfolded molecules were shown to exist in equilibrium.[39] However, the single-molecule experiments as well as the unfolding transition curves detected by NMR spectroscopy only provide information about the unfolding equilibrium in the presence of significant urea concentrations, and the linear free energy relationship is needed to obtain $\Delta G°(H_2O)$ values from these data.[40] Proton exchange experiments, in contrast, directly report on opened and closed states under native conditions.[41] Even minorities of partially unfolded forms in the native-state ensemble can thus be identified, presuming that they form faster than global unfolding takes place. In accordance with MD simulations[24] and the recently observed ring-flipping dynamics of F56 in the core of barstar-pWT,[25] the proton-exchange reactions of this variant were found to occur in the microseconds to seconds time domain (Figure 3A and B). This observation indicates an extensive dynamic heterogeneity within the native-state ensemble. With the exception of E8 and G43, none of the ΔG_{HX} values agrees with the global stability of 12.1 ± 1.6 kJ mol^{-1} (Figure 4) implying that the global unfolding transition of barstar-pWT is not mapped by these residues. This conclusion is further corroborated by the fact that none of these 20 amide protons show k_{op} values (Table S2) close to the unfolding rate constant found for the major unfolding phase ($\lambda_{1,u}^0 = 0.36 \pm 0.04$ s^{-1}). Since a correlation between the ΔG_{HX} values and secondary structural elements is not obvious (Figure 4), one might conclude that the native-state dynamics are dominated by uncooperative fluctuations. However, the 20 experimentally observed closing rate constants k_{cl} are distributed bimodal (Figure 3D). This clustering of k_{cl} values into two groups might reflect the presence of cooperative closing processes starting

(39) Hofmann, H.; Golbik, R. P.; Ott, M.; Hübner, C. G.; Ulbrich-Hofmann, R. *J. Mol. Biol.* **2008**, *376*, 597–605.
(40) Myers, J. K.; Pace, C. N.; Scholtz, J. M. *Protein Sci.* **1995**, *4*, 2138–2148.
(41) Teilum, K., Kragelund, B. B., Poulsen, F. M. *Application of hydrogen exchange kinetics to studies of protein folding*. Wiley-VCH: Weinheim, 2005; Vol. 2, pp 635−672.

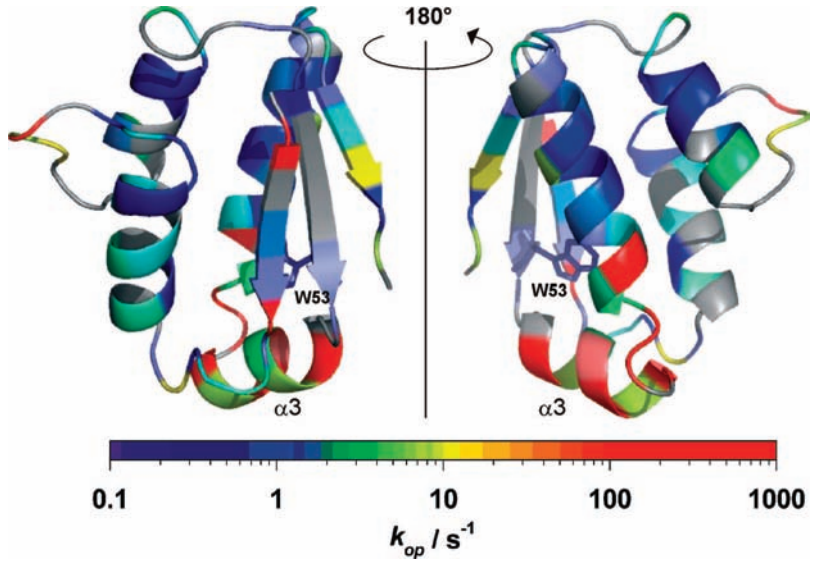

Figure 7. Mapping of k_{op} (color coded) to the tertiary structure of barstar. The side chain of W53 is depicted by a stick representation. The structure was taken from the protein database (pdb-file: 1bta).

from molecules with an enhanced solvent accessible surface area. Uncooperative fluctuation, in contrast, should lead to a unimodal broad distribution of k_{cl} values since the closing reactions of amide protons at different positions of the molecule should be completely uncorrelated. Large variations in the closing rate constants were also described for other proteins,[23,42−44] indicating that heterogeneous open-state ensembles reflect a general feature of proteins.

Similar to the closing process, the opening rate constants for 64 amino acid residues vary by a factor of more than 100 along the amino acid sequence (Figure 3C). An at least bimodal spectrum of k_{op} values (Figure 3C) indicates again the presence of cooperative opening events. In Figure 7 the k_{op} values are mapped onto the NMR structure of barstar illustrating the extensive dynamics of helix 3 and the adjacent loop, which is reflected in high closing rate constants as well. This observation suggests that helix 3 and the adjacent loop represent an unstable hot spot of the protein with mean rate constants of $\langle k_{op} \rangle = 20 \pm 6$ s^{-1} and $\langle k_{cl} \rangle = 656 \pm 310$ s^{-1} (Q58−S69) (errors are standard errors for the k_{op} values and k_{cl} values in Table S2). Hence, in equilibrium a minority of all molecules sojourn in a high-energy state having a distorted or even unstructured helix 3. Depending on the solvent accessibility of the amide protons, the k_{op} values in helix 3 itself fluctuate periodically along the sequence (Figure 3, Table S2). Therefore, the mean k_{op} value provides only a rough estimation about the opening process of the complete helix. However, although helix 3 covers the hydrophobic core of barstar, shielding it from solvation, the dynamics of the helix, even on positions close to the hydrophobic core, seem to be completely decoupled from the global unfolding process. This conclusion is in accordance with the result of a ϕ-value analysis of this protein,[28] showing helix 3 to be only very weakly formed in the two transition states on the route from unfolded to native molecules.

Interestingly, the native-state dynamics data can be related to the rates of the unfolding reaction observed in stopped-flow fluorescence experiments (Figures 3 and 6). Mechanistically, the unfolding of barstar was previously shown to proceed via two intermediates, populated on parallel pathways during the dead time (1 ms) of a stopped-flow instrument.[30] In our studies on barstar-pWT one unfolding intermediate could be directly detected via the fast unfolding reaction with the rate constant λ_2. From the similarity of $\lambda_{2,u}{}^0$ at 0 M urea (9.9 ± 1.2 s^{-1}) and the opening rate constants in helix 3 ($\langle k_{op} \rangle = 20 \pm 6$ s^{-1}), it can be concluded that helix 3 is in the exchange-competent form in this intermediate and, therefore, most likely unstructured. This in turn might lead to the solvation of the hydrophobic core of barstar-pWT and thus to a change in the fluorescence of W53 being close to helix 3. Although it is beyond the score of this work to present a complete mechanism for the unfolding of barstar-pWT, the free energy difference between the unfolding intermediate and the native state is accessible from the stopped-flow fluorescence experiments. From the rate constants of fast folding ($\lambda_{2,f}{}^0 = 296 \pm 224$ s^{-1}) and unfolding ($\lambda_{2,u}{}^0 = 9.9 \pm 1.2$ s^{-1}) under native conditions (Figure 6), a free energy difference between the native state and the intermediate of 8.4 ± 1.9 kJ mol^{-1} is obtained. In comparison, the free energy difference between the opened and closed conformation of helix 3 and its adjacent loop (Q58, K60, Q61, L62, N65, G66, E68, and S69) is accessible from the ΔG_{HX} values (Figure 4; Table S2), giving a mean value of $\langle \Delta G_{HX} \rangle = 7.5 \pm 0.7$ kJ mol^{-1}. Within the error (standard error of the ΔG_{HX} values in Table S2) this stability difference agrees with that calculated from the rate constants for the fast folding and unfolding reaction (8.4 ± 1.9 kJ mol^{-1}), which further corroborates the conclusion that the fast proton exchange kinetics of the residues in helix 3 and the fast unfolding reaction observed in the stopped-flow fluorescence experiments probe the same structural transition. These considerations lead to a free energy scheme with three structurally different states (N, I, U) (Figure 8A). Based on $\langle \Delta G_{HX} \rangle$, the high-energy state (I) of barstar-pWT is populated to 4.8 ± 1.4% under native conditions.

Depending on their time scale, the extensive dynamics of a protein native state is often reflected in high b-factors of its X-ray structure or in high rmsd values of the ensemble of energy minimized NMR structures as well. Helix 3 and its adjacent loop display high b-factors in the variant C82A[46] and high rmsd

(42) Kragelund, B. B.; Heinemann, B.; Knudsen, J.; Poulsen, F. M. *Protein Sci.* **1998**, *7*, 2237–2248.
(43) Arrington, C. B.; Robertson, A. D. *Biochemistry* **1997**, *36*, 8686–8691.
(44) Houliston, R. S.; Liu, C.; Singh, L. M.; Meiering, E. M. *Biochemistry* **2002**, *41*, 1182–1194.

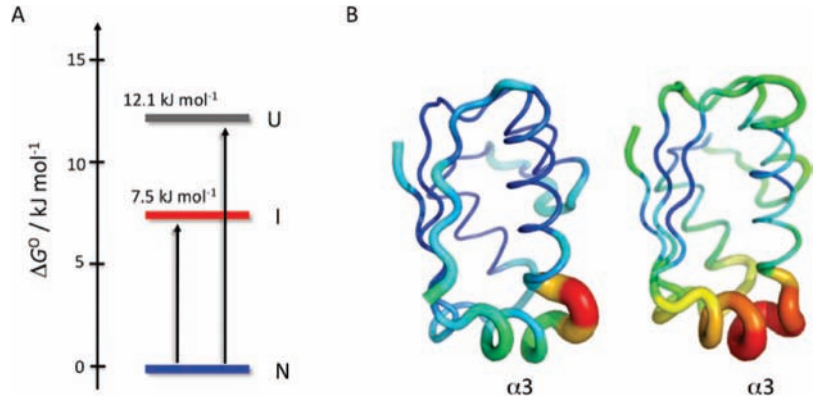

Figure 8. Free energy scheme as well as NMR and X-ray structures of barstar. (A) Free energies of the native state (N), the intermediate state with exchange competent helix 3 (I), and the unfolded state (U). (B) NMR structure of the wildtype protein (right, pdb-file: 1bta) and X-ray structure of the variant C82A (pdb-file: 1A19). The rmsd values and the b-factors are coded by the thickness in the sausage representation.

values in the NMR structure of the wildtype protein[45] (Figure 8B), which is in line with our results. The accordance of the results of four different techniques (native-state proton-exchange, X-ray-crystallography, NMR-spectroscopy, and stopped-flow fluorescence spectroscopy) clearly indicates a close coupling between the native-state dynamics of barstar and its unfolding pathway. Obviously, the native-state ensemble of this protein samples a large conformational space thereby populating a high-energy state with a disturbed helix 3 which is, under nonequilibrium conditions, observable as a distinct unfolding intermediate.

4. Materials and Methods

4.1. Protein Expression and Purification. The protein expression host *E. coli* JM109 was transformed with the plasmid pKK223-3 containing an ampicillin resistance and the oligonucleotide sequence of pWT.[28] Protein expression and purification were performed as reported elsewhere.[16]

4.2. Urea Induced Unfolding Transition with 2D ^{15}N-TROSY-HSQC Spectra. 2D ^{15}N-TROSY-HSQC spectra of 1 mM ^{15}N-barstar-pWT were acquired on a Bruker Avance 600 at 298 K in 50 mM sodium phosphate buffer, pH 8.0, containing 10% D_2O. The NMR spectra of two samples, one in pure buffer and one containing 5 M urea, were recorded. Afterward, defined aliquots of both samples were mixed to obtain the NMR spectra at intermediate urea concentrations. The equilibration time was 10 min. Spectra were processed using NMRPipe[47] and analyzed in NMRView.[48] The urea induced transition curves for the corresponding residues were obtained by plotting the cross-peak volumes as a function of the urea concentration. All urea induced unfolding transitions were fitted according to the two-state model.[49]

4.3. Fast Proton Exchange Using an MEXICO Pulse Sequence. The rate constants for proton exchange were determined from 2D ^{1}H$-^{15}$N NMR correlation spectra using a modified MEXICO pulse sequence[31] on a Bruker Avance 500 (for pH 6.5, 7.0, 8.0) and a Bruker Avance 600 (for pH 9.0, 10.0) at 298 K in 50 mM sodium phosphate buffer. This sequence dephases transversal magnetization of the amides, whereas the magnetization of water protons relaxes back to +Z by radiation damping. Amide cross peaks reappear due to back exchange of this water magnetization, and the volumes of these resonances at different exchange periods were used to determine the rate constant for proton exchange (k_{HX}) using

$$S = \left(\frac{k_{\mathbf{HX}}}{R_1 + R_w}\right) \cdot \{\exp[-R_w \cdot t] - \exp[-(R_1 + k_{HX}) \cdot t]\} \tag{3}$$

with S corresponding to the volume of the crosspeaks relative to a reference spectrum, R_1 to the relaxation rate constant of the amide protons, R_w to the relaxation rate constant of water protons, and t to the exchange time. R_w was determined to be 0.42 s^{-1}.

4.4. Kinetic Single- and Double-Mixing Experiments by Stopped-Flow Fluorescence Spectroscopy. Kinetic experiments were performed on an Applied Photophysics SX-20MV stopped-flow instrument at 298 K. An excitation wavelength of 280 nm was used, and the fluorescence above 320 nm was collected. All experiments were performed in 50 mM sodium phosphate buffer, pH 8. Unfolding experiments were performed by mixing the protein (55 μM) with 10 volumes of buffer containing urea at different concentrations.

Refolding experiments were performed by mixing the unfolded protein (55 μM, 5 M urea) with 10 volumes of buffer solution containing the corresponding concentration of urea. The final protein concentration was 5 μM. Double-mixing experiments were used to determine the refolding from the unfolded protein having the peptidyl−prolyl bond Y47−P48 in a *cis*-conformation. First, the protein was unfolded for 3 s at 4.3 M urea resulting in an unfolded protein with the peptidyl−prolyl bond Y47−P48 in a *cis*-conformation.[17] Refolding was initiated by a second jump to the refolding buffer containing the corresponding urea concentration. The final protein concentration was 2 μM. The refolding kinetics was fitted with a single-exponential function, whereas a double exponential function was used to fit the unfolding kinetics. The chevron plots were fitted according to

$$\lambda_1 = \lambda^0_{1,u} \exp(m_{1,u}[\text{urea}]) + \lambda^0_{1,f} \exp(m_{1,f}[\text{urea}] + m'_{1,f}[\text{urea}]^2) \tag{4}$$

$$\lambda_2 = \lambda^0_{2,u} \exp(m_{2,u}[\text{urea}]) + \lambda^0_{2,f} \exp(m_{2,f}[\text{urea}]) \tag{5}$$

where $m_{1,u}$ and $m_{1,f}$, $m_{1,f}'$ are the slopes of the corresponding chevron limbs for unfolding and refolding of the slow phase and $m_{2,u}$ and $m_{2,f}$ the slopes of the chevron limbs for the fast phase. $\lambda_{1,f}^0$ and $\lambda_{1,u}^0$ are the rate constants of the slow phase extrapolated to 0 M urea, and $\lambda_{2,f}^0$ and $\lambda_{2,u}^0$ are the rate constants of the fast phase at 0 M urea.

Acknowledgment. We thank Prof. Benjamin Schuler for critical reading of the manuscript and the Max-Planck Research Unit for

(45) Lubienski, M.,J.; Bycroft, M.; Freund, S. M.; Fersht, A. R. *Biochemistry* **1994**, *33*, 8866–8877.
(46) Ratnaparkhi, G. S.; Ramachandran, S.; Udgaonkar, J. B.; Varadarajan, R. *Biochemistry* **1998**, *37*, 6958–6966.
(47) Delaglio, F.; Grzesiek, S.; Vuister, G. W.; Zhu, G.; Pfeifer, J.; Bax, A. *J. Biomol. NMR* **1995**, *6*, 277–293.
(48) Johnson, B. A. *Methods Mol. Biol.* **2004**, *278*, 1505–15014.
(49) Clarke, J.; Fersht, A. R. *Biochemistry* **1993**, *32*, 4322–4329.

Enzymology of Protein Folding, Halle (Germany) for providing the Bruker Avance 500 instrument for NMR measurements and the Graduiertenkolleg 1026 of the German Research Foundation (Bonn, Germany) for intellectual and financial support. Moreover, the German National Academic Foundation (Bonn, Germany) and the Max-Buchner Foundation (Frankfurt/Main, Germany) are gratefully acknowledged for financial support for H.H.

Supporting Information Available: . The stability of barstar-pWT as function of pH and the rate constants for folding and unfolding at three pH values (8, 9, 10) are shown in Figure S1. Examples of ^{15}N-HSQC-NMR spectra at different exchange times and exchange kinetics for residue K2 at five pH values are presented in Figure S2. The stability parameters for the urea induced transition curves detected by ^{15}N-TROSY/HSQC-NMR and the exchange rate constants as well as the deduced k_{op} and k_{cl} values are shown in Tables S1 and S2. This material is available free of charge via the Internet at http://pubs.acs.org.

JA8048942